

Article

Biochar from Lemon Stalks: A Highly Active and Selective Carbocatalyst for the Oxidation of Sulfamethoxazole with Persulfate

Spyridon Giannakopoulos¹, John Vakros^{1,2,*}, Zacharias Frontistis³, Ioannis D. Manariotis⁴, Danae Venieri⁵, Stavros G. Pouloupoulos⁶ and Dionissios Mantzavinos¹

¹ Department of Chemical Engineering, University of Patras, Caratheodory 1, University Campus, GR-26504 Patras, Greece

² School of Sciences and Engineering, University of Nicosia, Nicosia 2417, Cyprus

³ Department of Chemical Engineering, University of Western Macedonia, GR-50132 Kozani, Greece

⁴ Environmental Engineering Laboratory, Department of Civil Engineering, University of Patras, University Campus, GR-26504 Patras, Greece

⁵ School of Chemical & Environmental Engineering, Technical University of Crete, GR-73100 Chania, Greece

⁶ Department of Chemical and Materials Engineering, School of Engineering and Digital Sciences, Nazarbayev University, Astana 010000, Kazakhstan

* Correspondence: vakros@chemistry.upatras.gr

Abstract: Pyrolysis of lemon stalks at 850 °C under a limited oxygen atmosphere yields a highly active and selective biochar for the activation of persulfate ion and the oxidation of sulfamethoxazole (SMX). The biochar mainly consists of C and O atoms, with Ca and K being the most abundant minerals. It has a moderate specific surface area of 154 m² g⁻¹ and carbonate species, probably in the form of calcium carbonate. Complete degradation of 0.5 mg L⁻¹ SMX can be achieved within 20 min using 500 mg L⁻¹ sodium persulfate (SPS) and 100 mg L⁻¹ biochar in ultrapure water (UPW). The acidic environment positively influences the degradation and adsorption processes, while the complexity of the water matrices usually has a negative impact on the degradation. The presence of chloride accelerates the oxidation of SMX, whose mechanism follows radical and non-radical pathways. Hydroxyl radicals seem to have the dominant contribution, while the electron transfer pathway was proven with electrochemical characterization. The biochar is stable for at least five cycles, and this makes it a good candidate for a sustainable, metal-free catalyst.

Keywords: biochar; sulfamethoxazole; persulfate; electron transfer



Citation: Giannakopoulos, S.; Vakros, J.; Frontistis, Z.; Manariotis, I.D.; Venieri, D.; Pouloupoulos, S.G.; Mantzavinos, D. Biochar from Lemon Stalks: A Highly Active and Selective Carbocatalyst for the Oxidation of Sulfamethoxazole with Persulfate. *Catalysts* **2023**, *13*, 233. <https://doi.org/10.3390/catal13020233>

Academic Editor: Hui Zhang

Received: 27 December 2022

Revised: 9 January 2023

Accepted: 16 January 2023

Published: 19 January 2023



Copyright: © 2023 by the authors. Licensee MDPI, Basel, Switzerland. This article is an open access article distributed under the terms and conditions of the Creative Commons Attribution (CC BY) license (<https://creativecommons.org/licenses/by/4.0/>).

1. Introduction

Wastes from wastewater treatment plants (WWTPs), hospitals, agriculture, and farms are likely to contain various antibiotics, sometimes at high concentrations, since these pharmaceuticals are widely used in various activities; such wastes may end up in the environment such as rivers, surface waters, and the sea. In fact, many antibiotics are resistant to degradation and mineralization in WWTPs due to their complex chemical structures. It is important to note that in areas with high levels of contamination, these chemicals can remain in the environment due to their physicochemical properties, making certain bacteria resistant to antibiotics. This can lead to the natural environment becoming a pool of antibiotic-resistant pathogens, which under certain conditions can enter the food chain and create antibiotic-resistant microbes that pose a threat to human health [1].

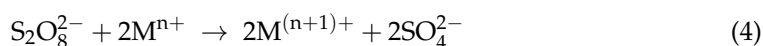
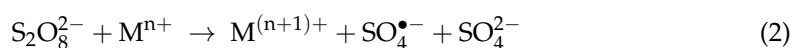
Sulfonamides is one of the most common families of antibiotics with sulfamethoxazole (SMX) being a typical representative. They are typically found in terrestrial and aqueous matrices [2–4], mainly due to their high resistance to soil and use in excessive quantities [5]. For instance, detection of sulfonamides has been reported in 80% of 139 rivers and streams sampled in 1999–2000 in 30 states in the US [6]. From that period onwards, sulfonamides

are found in livestock-related rivers, agro-industrial streams [7–9], and wetlands and surface waters [10]. Although antibiotics are present in surface waters at concentrations of ng L^{-1} [11,12], maximum concentration values in rivers in the order of $\mu\text{g L}^{-1}$ have also been reported [13,14]. More specifically, SMX was detected in all samples from river Seine, France at a maximum concentration of 544 ng L^{-1} [15]. The occurrence of SMX at concentrations up to $1 \mu\text{g L}^{-1}$ was reported in 20% of groundwater samples during a monitoring campaign in the US [16].

Therefore, there is a need to develop efficient technologies to adequately remove persistent pollutants, such as SMX, which are not fully degraded in conventional WWTPs [17,18]. In recent decades, advanced oxidation processes (AOPs) have evolved as promising treatment technologies based on the production of reactive oxygen species (ROS) that completely oxidize organic pollutants into end products such as water, carbon dioxide, and minerals. ROS mainly involve radicals that are essentially derived from an ion, molecule or atom having at least one unpaired electron in the outer electron layer. Due to such an electronic configuration, a free radical becomes very active as it is very unstable and can react rapidly with several types of organic pollutants [19]. Hydroxyl radicals, which perhaps are the most common ones, can be produced from the reaction of hydrogen peroxide with iron ions in acidic conditions [20]. In the past few years, sulfate radicals have become a good alternative to hydroxyl radicals [21] since they are more selective for the oxidation of organic molecules by electron transfer [22]. Persulfate ions, $\text{S}_2\text{O}_8^{2-}$, have an O–O bond with length proportional to that in H_2O_2 [23,24] but exhibit higher water solubility and stability [25] than H_2O_2 . The redox potential of $\text{S}_2\text{O}_8^{2-}$ is 2.01 V, but it requires an activator to produce sulfate radicals:



Activation can be performed with heat [26], ultrasound [27], solar or UV irradiation [28], and in the presence of a transition metal [29–31], i.e., Equations (2)–(4):



In the last decade, metal-free catalysis has gained considerable attention. Carbonaceous materials, such as biochar (BC), can be used for the activation of persulfate. Pyrolysis of waste biomass yields BC with moderate to high specific surface area (SSA), hierarchical pore structure, and plenty of surface functional groups. Biochar find significant applications as supercapacitors [32], adsorbents [33], catalysts in transesterification reactions [34], and persulfate activators to oxidize emerging contaminants. They can be prepared from any kind of raw biomass and their properties; for instance, aromaticity and the polarity index depend on the nature and type of oxygenated functional groups formed on the surface [35–37], which is a function of the pyrolysis conditions and the characteristics of raw biomass.

A type of biomass that is found in abundance worldwide is the trimmings of citrus and fruit trees, containing high levels of lignin and cellulose but low humidity. All over the world, there are large areas with orchards where fruit trees are grown such as orange, lemon, pear, apple, and so on. Due to the need for regular care of these arable lands through annual pruning of the trees, very large quantities of unwanted wood (trunks, branches, stalks) and leaves are obtained [38], which are most often burned. For instance, the annual production of lemons for the period 2019–2020 was estimated at 7.55 million metric tons, with Mexico holding first place with 2.2 million metric tons, followed by the European Union and Argentina with 1.42 and 1.4 million tons, respectively [39].

In this work, biochar prepared from lemon stalk was used to activate persulfate for the destruction of SMX. To our knowledge, this is the first time that this kind of biomass

was employed for the production of BC, which was then applied for SMX oxidation. Previous studies have dealt with SMX oxidation through the carbocatalytic activation of persulfate with various biochar from spent coffee grounds [40], olive stones [41], spent malt rootlets [42], and rice husks [43]. In general, agro-industrial BC is an excellent persulfate activator for SPS and the subsequent degradation of antibiotics. In this perspective, a new BC was synthesized, characterized with different physicochemical techniques, and tested for the degradation of SMX. Electrochemical characterization was applied to elucidate the degradation mechanism.

2. Results and Discussion

2.1. Biochar Characterization

The SEM image (Figure 1) shows that there are some crystallites formed on the surface of carbon phase. These crystallites have relatively long dimensions and are rich in Ca, as was shown from the EDX analysis.

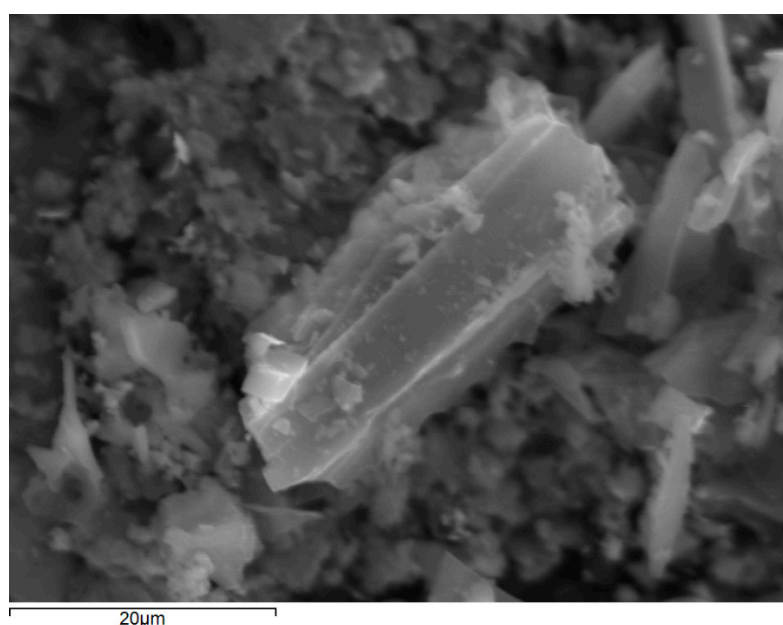


Figure 1. Representative SEM image of the biochar showing deposits of minerals.

The formation of carbonate species may either be due to pyrolysis or, more likely, the exposure of BC in the air and the subsequent reaction of CaO with CO₂. Based on EDX analysis, the percent elemental composition was as follows: 86.5% C, 12.2% O, 0.5% Ca, 0.3% K, 0.2% Mg, and 0.1% from each of P, Si, and Cl. Minerals were in the form of oxides and carbonates, since only small amounts of Cl were detected.

The XRD pattern (Figure 2) exhibits two broad peaks centered at 2 θ about 23° and 43.6°, which are typical of the graphitization process during pyrolysis. The broad peak at 23° refers to graphitic carbon and is due to the (002) plane. The second peak describes the (100) plane of the sp² hybridization of the carbon atoms [44,45]. There are some other sharp peaks centered at 26.5° and 29.4° due to carbonate minerals such as calcite, in accordance with the EDX analysis. Their content is rather limited, and the sharp peak indicates the absence of significant interactions with the carbon phase.

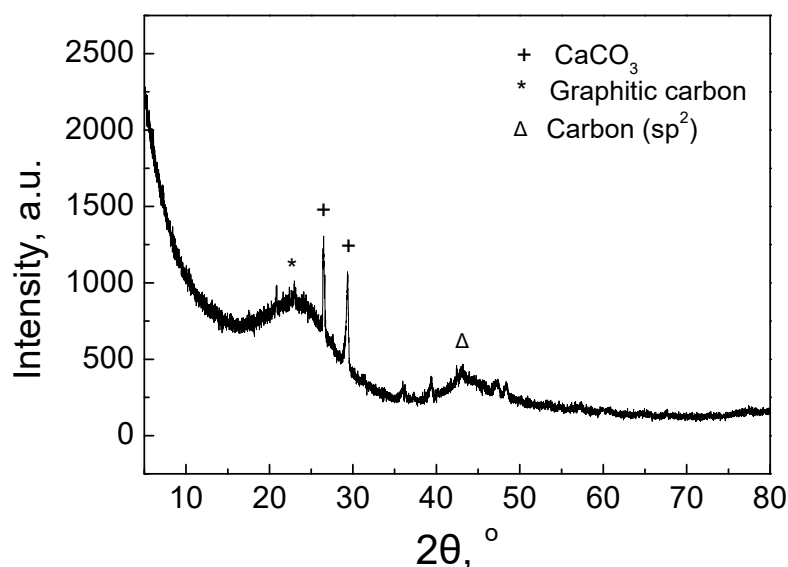


Figure 2. XRD pattern of the biochar.

As can be seen in the FTIR spectrum (Figure 3), there is a broad peak centered at 3430 cm^{-1} and a peak at 1105 cm^{-1} . These peaks are due to -OH and C-O(H) bonds and refer to the surface hydroxyl species and/or adsorbed water molecules. The peak at 1432 cm^{-1} is due to the carbonate species, probably closely related with Ca (or K) ions, while the 1631 cm^{-1} describes the C=C bonds. There also are two peaks at 2917 and 2845 cm^{-1} , which are due to C-H aliphatic bonds. The absence of any peak above 3000 cm^{-1} denotes that the aromatic phase is poor in H, since the C-H bonds in aromatic or unsaturated bonds generate peaks above 3000 cm^{-1} [41].

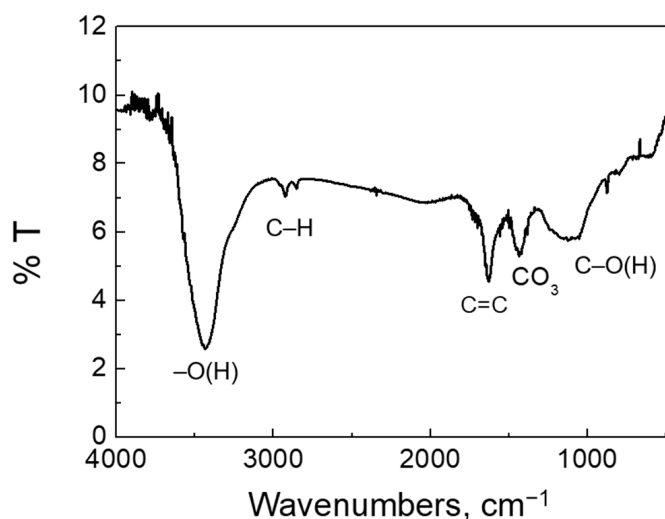


Figure 3. FTIR spectrum of biochar.

The TGA curve (Figure 4) clearly shows that the organic phase is highly homogeneous. There is a sharp decrease in mass starting at 450 °C , while the differential curve reveals that there is a sharp peak at 505 °C . Interestingly, the mass left after the TGA run is only 7%; therefore, the minerals content is limited in the biochar.

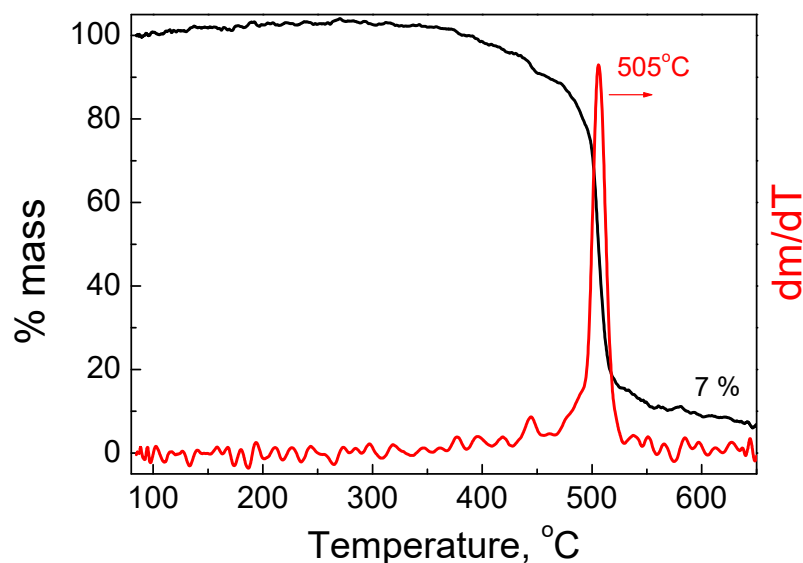


Figure 4. TGA (black line) and differential curve, dm/dT , (red line) of biochar. TGA was performed under air atmosphere at $10\text{ }^{\circ}\text{C min}^{-1}$ heating rate.

The SSA of the biochar was measured equal to $154\text{ m}^2\text{ g}^{-1}$. The micropores' SSA was $105\text{ m}^2\text{ g}^{-1}$, while the total pore volume was 0.08 mL g^{-1} . The pore width was about 1.9 nm , while some macropores were also present, as can be seen in Figure 5.

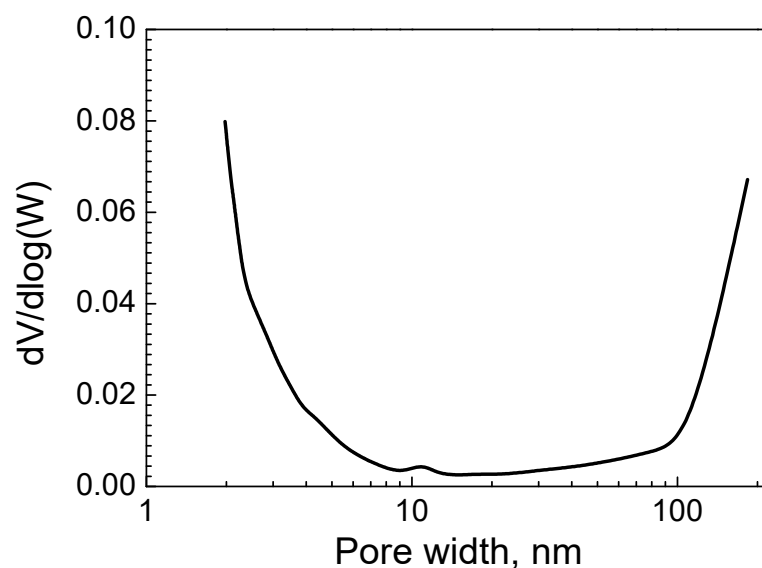


Figure 5. Pore width distribution of biochar.

The point of zero charge was determined using the potentiometric mass titration method [46] and it was found equal to 9.2. This value confirms the basic character of the biochar surface, which can be attributed to CaCO_3 .

2.2. Biochar Activity

2.2.1. Preliminary Screening Experiments

Figure 6 shows the extent of SMX removal by adsorption and oxidation during preliminary experiments with biochar produced from various lemon tree parts, i.e., leaves pyrolyzed at 400 or $850\text{ }^{\circ}\text{C}$ (LL400 or LL850), stalks (LST), and branches (LBR). SMX removal is mainly due to the oxidation process (Figure 6b), although adsorption contributes considerably in certain occasions (Figure 6a).

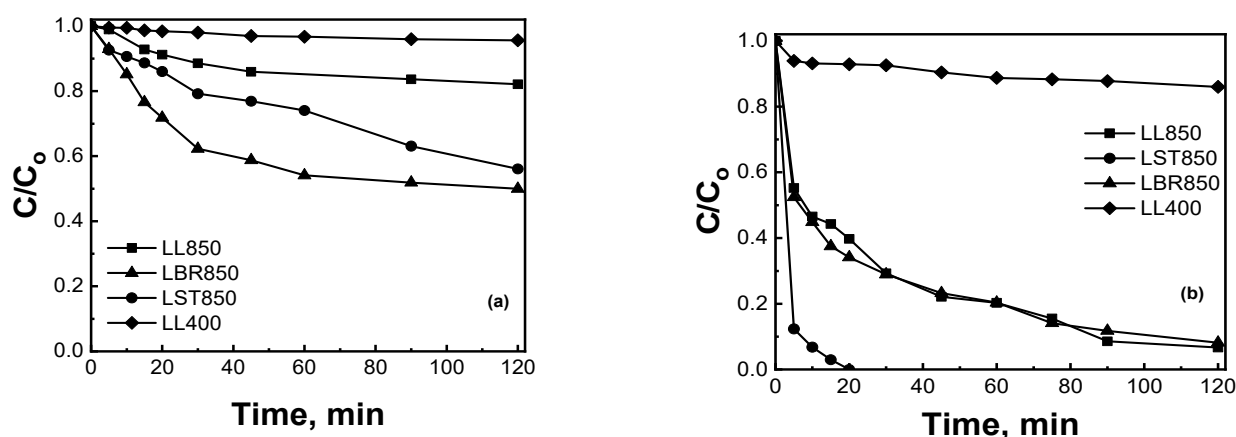


Figure 6. Removal of 0.5 mg L^{-1} SMX 100 mg L^{-1} BC under (a) adsorption and (b) oxidation with 500 mg L^{-1} SPS in UPW and inherent pH.

Adsorption is either due to interactions between opposite-charged species in the solution and surface functional groups (electrostatic adsorption) or π - π interactions between the organic contaminant and the graphitic phase [47]. As can be seen in Figure 6a, biochar prepared from biomass with higher lignin content exhibits greater adsorption capacity. Moreover, the pyrolysis temperature positively affects the degree of adsorption, probably due to higher graphitization levels occurring at higher temperatures. A similar trend regarding pyrolysis temperature occurs for the oxidation process (Figure 6b) and is consistent with previous studies [43]. SMX decomposition is complete within 20 min of the reaction with the biochar from stalks, while 90% can be achieved after 120 min with biochar from leaves or brunch.

Table 1 summarizes the conditions needed (i.e., biochar and persulfate concentrations and reaction time) to achieve maximum SMX degradation with various biochar tested in previous studies of our group. Evidently, the LST850 sample prepared in this work showed higher activity than previous materials in terms of reaction time and/or chemicals concentrations. In this respect, all subsequent experiments were performed with LST850. Figure 7 shows the effect of SPS, biochar, or initial SMX concentration on its degradation.

Table 1. Removal of SMX with biochar from different biomasses pyrolyzed at $850 \text{ }^\circ\text{C}$. Values with asterisks refer to an experiment with trimethoprim as the target compound.

Biomass	BC (mg L^{-1})	SPS (mg L^{-1})	Removal (%)	Time (min)	Reference
Coffee grounds	200	1000	97	75	[40]
Malt rootlets	90	250	94	90	[42]
		500 *	74 *	120 *	[48]
Olive stones	200	1000	65	75	[41]
Rice husks	100	500	96	120	[43]

* The values are refer to the degradation of trimethoprim instead of SMX.

The beneficial effect of increasing SPS concentration in the range of 0 – 500 mg L^{-1} on SMX degradation is presented in Figure 7a. Assuming that degradation follows a pseudo-first-order rate expression with regards to SMX concentration, apparent kinetic constants can be computed from the data of Figure 7a; the respective values are 0.0052 min^{-1} , 0.0581 min^{-1} , 0.0738 min^{-1} , 0.0938 min^{-1} , 0.1227 min^{-1} , and 0.2574 min^{-1} at 0 , 25 , 50 , 125 , 250 , and 500 mg L^{-1} SPS. Evidently, more radicals are produced at higher oxidant source concentrations, and this may possibly offset the competition between SMX and SPS for adsorption on the biochar's active sites. It should be noted here that excessive oxidant concentrations may be detrimental to the process due to radical scavenging effects and/or the conversion of sulfate and hydroxyl radicals to less powerful species such as $\text{S}_2\text{O}_8^{\bullet-}$.

and O₂ [49]; this effect was not observed at the maximum SPS concentration employed in this work.

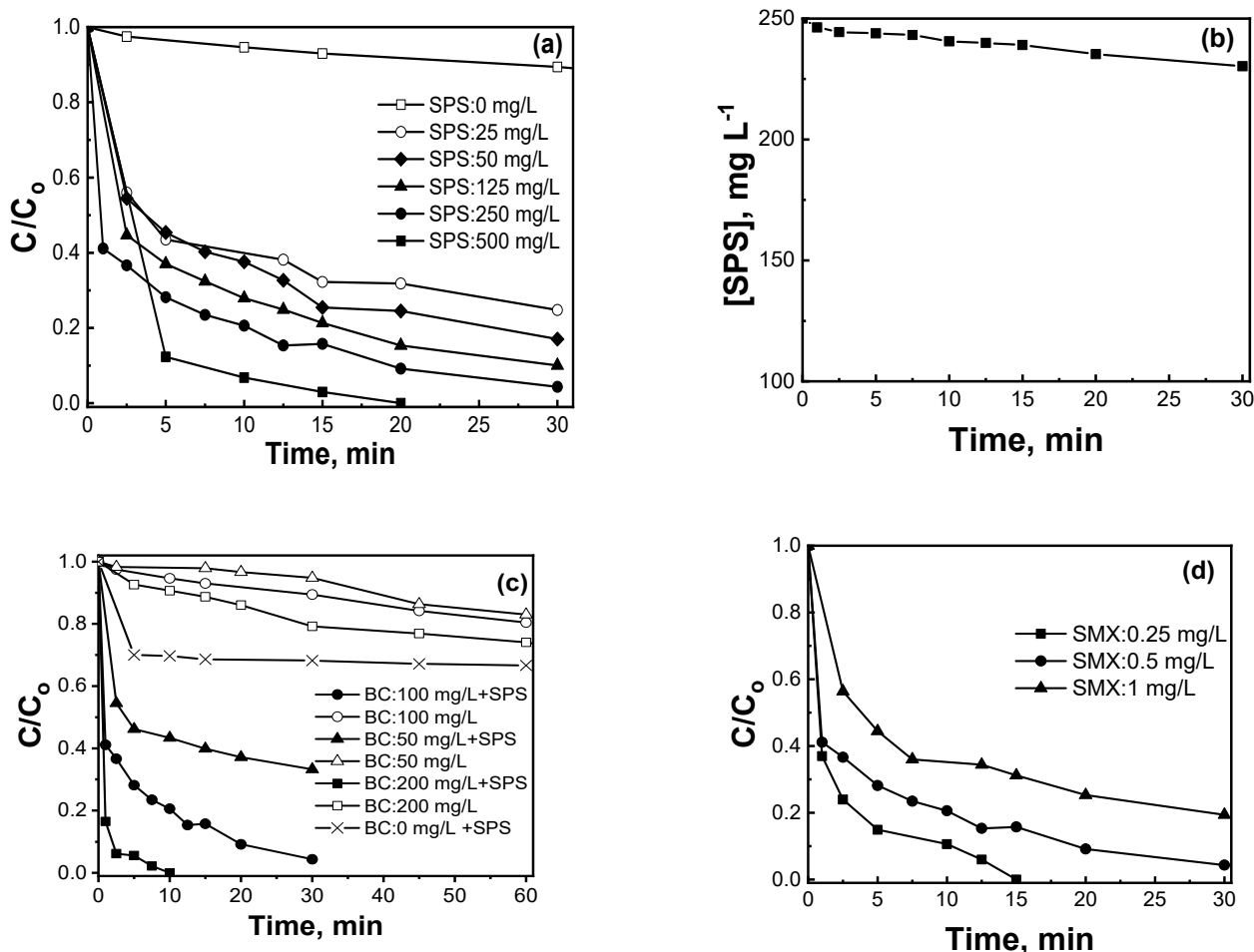


Figure 7. Removal of SMX in UPW and inherent pH as a function of (a) SPS concentration (0.5 mg L⁻¹ SMX and 100 mg L⁻¹ BC), (b) shows SPS consumption with 100 mg L⁻¹ BC, (c) BC concentration (0.5 mg L⁻¹ SMX with and without 250 mg L⁻¹ SPS), and (d) SMX concentration (100 mg L⁻¹ BC and 250 mg L⁻¹ SPS).

Subsequent experiments were performed at 250 mg L⁻¹ SPS in order to (i) keep the final concentration of sulfate ions in the treated effluent as low as possible and (ii) deliberately prolong the reaction time to make discrepancies in activity more readily observable. Interestingly, SPS was only partially converted to sulfate radicals and ions, as can be seen in Figure 7b; however, the concentration of radicals related to the 30-min SPS conversion of 8% sufficed to degrade SMX.

The positive effect of increasing biochar concentration in the range 0–200 mg L⁻¹ on the adsorption and oxidation of 0.5 mg L⁻¹ SMX is depicted in Figure 7c. Notably, SPS alone in the absence of biochar resulted in 30% SMX degradation in 60 min; this is because SPS is a mild oxidant on its own. However, the coexistence of persulfate and biochar is clearly beneficial since persulfate is activated, producing reactive oxygen species on the biochar surface and/or at the interfacial region or accelerating the transfer of electrons from organic molecules through the biochar's organic lattice. The apparent rate constants took values of 0.046 min⁻¹, 0.1227 min⁻¹, and 0.546 min⁻¹ at 50, 100, and 200 mg L⁻¹ of biochar, respectively.

The effect of SMX concentration in the range 0.25–1 mg L⁻¹ is depicted in Figure 7d; conversion decreases with increasing SMX concentration with the apparent rate constants being equal to 0.0682 min⁻¹, 0.1227 min⁻¹, and 0.2483 min⁻¹ at 1, 0.5, and 0.25 mg L⁻¹ SMX, respectively. Although data fitting to a first-order rate expression is good and allows

the computation of rate constants, the reaction is not true first order since the rate constant depends on the initial concentration.

2.2.2. Effect of pH

The solution pH strongly influences the surface charge of biochar, the form of SMX, and the activity of radicals. In this view, experiments were performed at initial pH values varying between 3 and 9 to study the effect of pH on adsorption and oxidation, and the results are shown in Figure 8. SMX adsorption was maximized at pH = 3 reaching 84% removal in 30 min, while it was considerably lower at pH = 7 (29%) and 9 (19%). The biochar whose pzc is 9.2 had its surface positively charged in a wide pH range. On the other hand, SMX has two pKa values of 1.4 and 5.7, while its isoelectric point is 4.5 [40,50]; this means that SMX is negatively charged at pH > 5.7 and neutral at 1.4 < pH < 5.7.

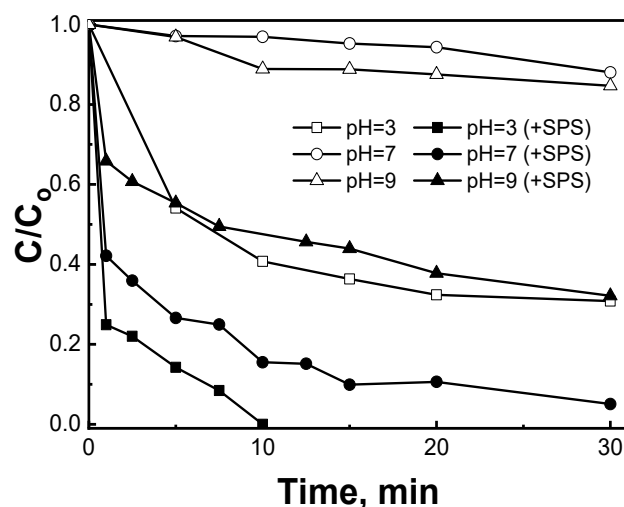


Figure 8. Effect of initial solution pH on the removal of 0.5 mg L⁻¹ SMX in UPW with 100 mg L⁻¹ biochar and in the presence or absence of 250 mg L⁻¹ SPS.

This explains the high level of SMX adsorption at pH = 3, where the biochar exhibited the higher positive charge, and the lower adsorption values at pH = 7 and 9 where the surface was less acidic and close to neutral. On the addition of SPS, its activation is accompanied by the formation of HSO₄⁻, a moderate acid, thus reducing the solution pH. SMX oxidation is much faster than adsorption, thus proving the catalytic action of biochar. Interestingly, complete SMX degradation can be achieved in just 10 min at pH = 3.

2.2.3. Effect of the Water Matrix

All experiments so far were performed in UPW, which is an unrealistic aqueous matrix, free of impurities, particles, and organic and inorganic compounds. Therefore, it was decided to test the process in various environmental matrices to assess the effect of their complexity on SMX degradation. Figure 9 shows experiments in secondary treated wastewater (WW), river water (RW), bottled water (BW), and seawater (SW); with the exception of BW, where the rate of degradation is comparable to UPW, all other matrices resulted in reduced degradation. The occurrence of various non-target inorganic and organic species in environmental matrices gives competitive reactions with SMX for the generated radicals, as well as the surface active sites available for adsorption [51]. Reactions in WW may also be decreased by its alkaline pH value of 8.4, as is demonstrated in Figure 8. Reduced rates in SW may partially be attributed to the high salinity and the presence of high amounts of different inorganic ions and carbon. On the contrary, the presence in BW of cations like Ca²⁺, which interact positively with the catalyst surface and especially carbonate species, may explain the similar reactivities recorded in UPW and BW.

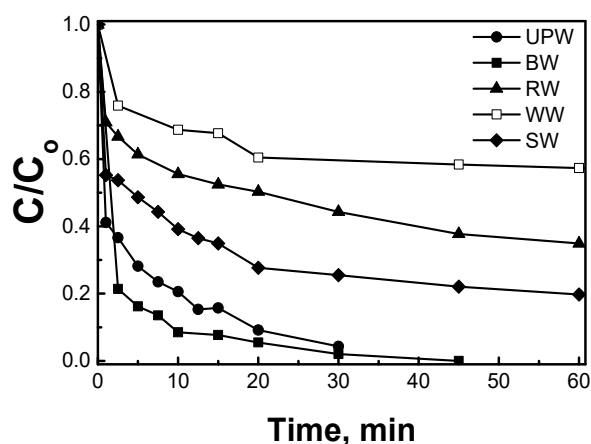


Figure 9. Effect of water matrix on the degradation of 0.5 mg L^{-1} SMX with 100 mg L^{-1} biochar and 250 mg L^{-1} SPS at inherent pH.

To shed more light on the influence of different matrix species, experiments were performed in UPW spiked with bicarbonate, chloride, or humic acid (HA), and the results are shown in Figure 10. Bicarbonate at 250 mg L^{-1} (i.e., concentration that matches that in BW and WW) has practically little effect, leading to 90% SMX degradation in 30 min. Although bicarbonate may scavenge sulfate and hydroxyl radicals, this is partially compensated by the formation of carbonate radicals, i.e., Equations (5) and (6):

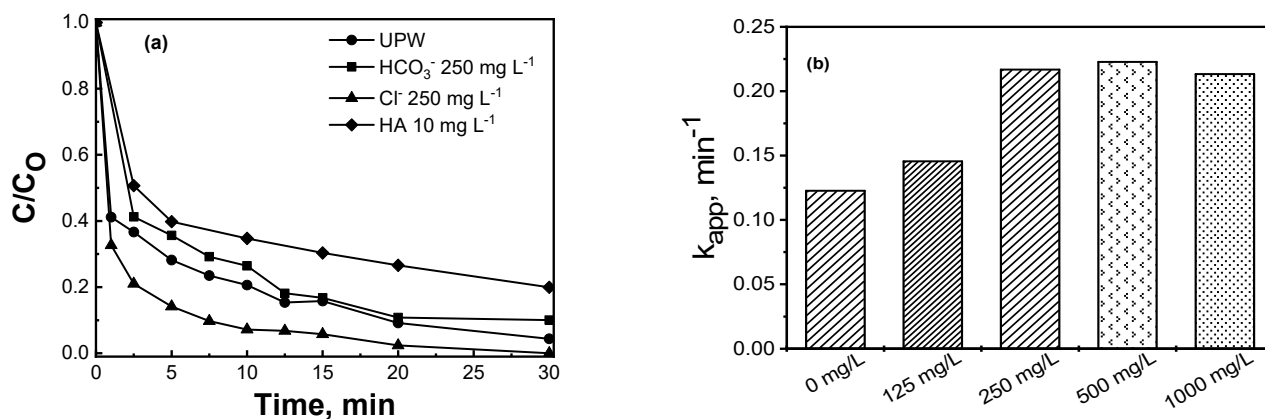
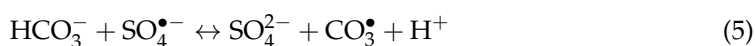


Figure 10. Degradation of 0.5 mg L^{-1} SMX with 100 mg L^{-1} biochar and 250 mg L^{-1} SPS in UPW and inherent pH as a function of (a) spiked chloride, bicarbonate, or humic acid; (b) Chloride spiked at various concentrations.

Interestingly, chloride at 250 mg L^{-1} favors SMX degradation; the computed apparent rate constant increased from 0.1227 min^{-1} in UPW to 0.2168 min^{-1} at 250 mg L^{-1} chloride and remained unchanged at concentrations up to 1000 mg L^{-1} (Figure 10b). This effect is ascribed to the formation of $\text{Cl}_2/\text{HOCl}/\text{Cl}^{\bullet}$ [52], which stimulate the reaction rate as described in Equations (7)–(9):



Although a large excess of Cl^- could intercept/interrupt the production of Cl^\bullet and facilitate the formation of the less reactive $\text{Cl}_2^{\bullet-}$, thus causing reduced rates [53], this has not been observed in this study for the range of chloride concentrations spiked in UPW; however, this effect may be associated with the reduced rate recorded in SW. Other studies have reported the formation of HOCl/Cl_2 through a mechanism of two-stage electron transfer [54] leading to the fast abatement of SMX and ciprofloxacin [55]. Also of interest is the reported reactivity of active chlorine species against organic pollutants having excess electron molecular moieties [56,57]. Moreover, enhanced reaction rates of pharmaceuticals have been related to the increased ionic strength induced by chloride [58]. Finally, the pair $\text{HO}^\bullet/\text{HOCl}^{\bullet-}$ (Equation (10)) may contribute to rate enhancement [59]:



Figure 10a also shows the detrimental effect of HA on SMX degradation; HA was spiked in UPW to simulate the natural organic matter typically found in waters, while its concentration was selected to match the organic carbon content of WW. Humic acid competes with SMX for either the surface active sites for adsorption and/or the precious oxidants, and this presumably decreases SMX degradation.

2.2.4. Effect of the Type of Pharmaceutical

To assess process applicability to treat other pharmaceuticals, the decomposition of losartan (LOS), valsartan (VAL), and dexamethasone (DEX) at initial concentrations of 0.5 mg L^{-1} was examined. LOS, primarily employed to treat high blood pressure, belongs to angiotensin receptor blockers. These compounds are partly metabolized and have been detected in wastewater treatment plants [60–62], hospital discharges [63], rivers [64], and seawater [65] at concentration levels from ng L^{-1} to $\mu\text{g L}^{-1}$. VAL, which is also used to regulate blood pressure [66], accumulates in the environment through feces and urine and has been detected in the natural ecosystem at concentration levels from ng L^{-1} to $\mu\text{g L}^{-1}$ [67,68]. DEX is a corticosteroid drug that is used to treat severe allergies, asthma, rheumatic problems, and skin diseases, amongst other diseases, and is mainly detected in the sewage of hospitals and pharmaceutical centers [69].

Figure 11 shows the relative reactivity of the four drugs, which decreases in the order: $\text{SMX} > \text{LOS} > \text{VAL} > \text{DEX}$. The ionization state of each compound plays an important role for the adsorption and oxidation, as has already been discussed in Section 2.2.2. The pK_a values of LOS, VAL, and DEX are 4, 3.6, and 1.2, respectively [66,70], which are lower than the upper value of SMX. This trend was followed in the degradation experiments, pointing out that the physicochemical properties of SMX favor its interactions with the biochar surface. Depending on the compound, the biochar can be more or less effective for its degradation. The selectivity of the biochar can be influenced by the speciation of the antibiotic. The acidity of the surface, and thus the solution pH, is one of the crucial parameters for the selectivity of the biochar in the oxidation of different antibiotics. This is the first evidence that oxidation is surface-sensitive and mainly occurs on the surface and interface of the biochar. In this respect, further experiments were performed to investigate possible mechanisms.

2.3. Degradation Mechanism

2.3.1. Electrochemical Characterization

In general, degradation of pollutants by AOPs can occur via different mechanisms including radical and non-radical pathways. To investigate the possible contribution of an electron transfer mechanism to SMX degradation, electrochemical measurements were performed [71], where the biochar was employed as an anodic electrode.

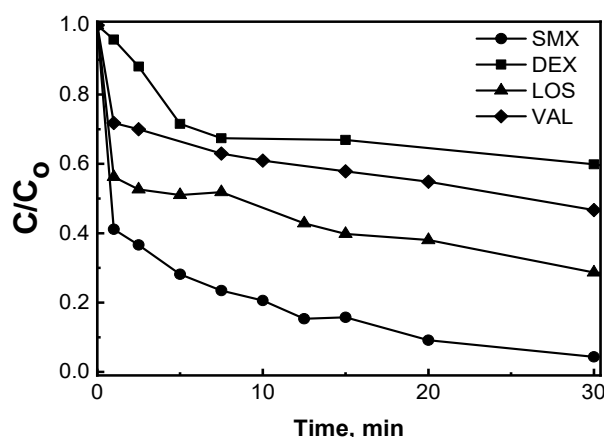


Figure 11. Degradation of 0.5 mg L^{-1} of various pharmaceuticals with 100 mg L^{-1} biochar and 250 mg L^{-1} SPS in UPW and inherent pH.

As depicted from the linear sweep voltammetry (LSV) curves (Figure 12a), the addition of 250 mg L^{-1} SPS to the solution (BC/SPS system) caused an increase in current density, indicating an interaction of SPS with the electrode surface due to the creation of metastable reactive complexes. A similar trend was recorded in the presence of 0.5 mg L^{-1} SMX (BC/SMX system), revealing charge flow between the organic molecule, which acts as an electron donor, and the electrode, and this possibly enhances degradation. A noteworthy current-density intensification was observed with the coexistence of the oxidant and the organic molecule (BC/SPS/SMX system), verifying the formation of an electron transfer pathway based on the establishment of a ternary interfacial complex between SMX, SPS, and BC surface groups. This increment in the charge transfer rate may be due to the easier and faster electron loss from the organic molecule towards the anode due to the redox potential change of the electrode in the presence of SPS, facilitating the direct oxidation of SMX by the biochar.

Then, an amperometry measurement was carried out, applying a voltage of 0 V (vs. Ag/AgCl) in the presence of $0.1 \text{ M Na}_2\text{SO}_4$ electrolyte in order to accurately determine the electron transfer between the catalyst, SPS, and SMX, as well as the direction of flow. According to Figure 12b, the addition of 250 mg L^{-1} SPS caused a dramatic current augmentation (from -0.25 mA to -1.4 mA), which is equivalent to a strong electron flow between the biochar and the oxidant and the function of SPS as an electron acceptor. In contrast, the following addition of 0.5 mg L^{-1} SMX resulted in a slight current decrease, thus revealing the electron displacement from the organic molecule to the BC/SPS complex, either to the carbonaceous surface, directly to the adsorbed SPS, or to the adsorbed SPS via the carbonaceous surface acting as an electron bridge. In this case, the possibility of the formation of a ternary complex, which favors electron transfer, can be supported [72].

In general, heterogeneous electron transfer is facilitated when the catalyst is characterized by high electrical conductivity. In this light, the charge transfer resistance (R_{CT}) of the material was examined using electrochemical impedance spectroscopy (EIS). The Nyquist plots for various conditions are given in Figure 12c, where the imaginary part of the impedance is represented as a function of its real part for the frequency range $0.1\text{--}10^5 \text{ Hz}$ by imposing a voltage of 0.2 V , which is sinusoidally perturbed with an amplitude of 0.01 V . In each curve, there is an incomplete semicircle whose diameter expresses the R_{CT} . Electrical conductivity is inversely proportional to the length of the diameter. When 250 mg L^{-1} SPS or 0.5 mg L^{-1} SMX are added, the diameter diminishes, equating to a greater mobility of charge carriers. In fact, when the oxidant and the organic molecule coexist, the resistance decreases further, confirming the charge flow in the BC/SPS/SMX system.

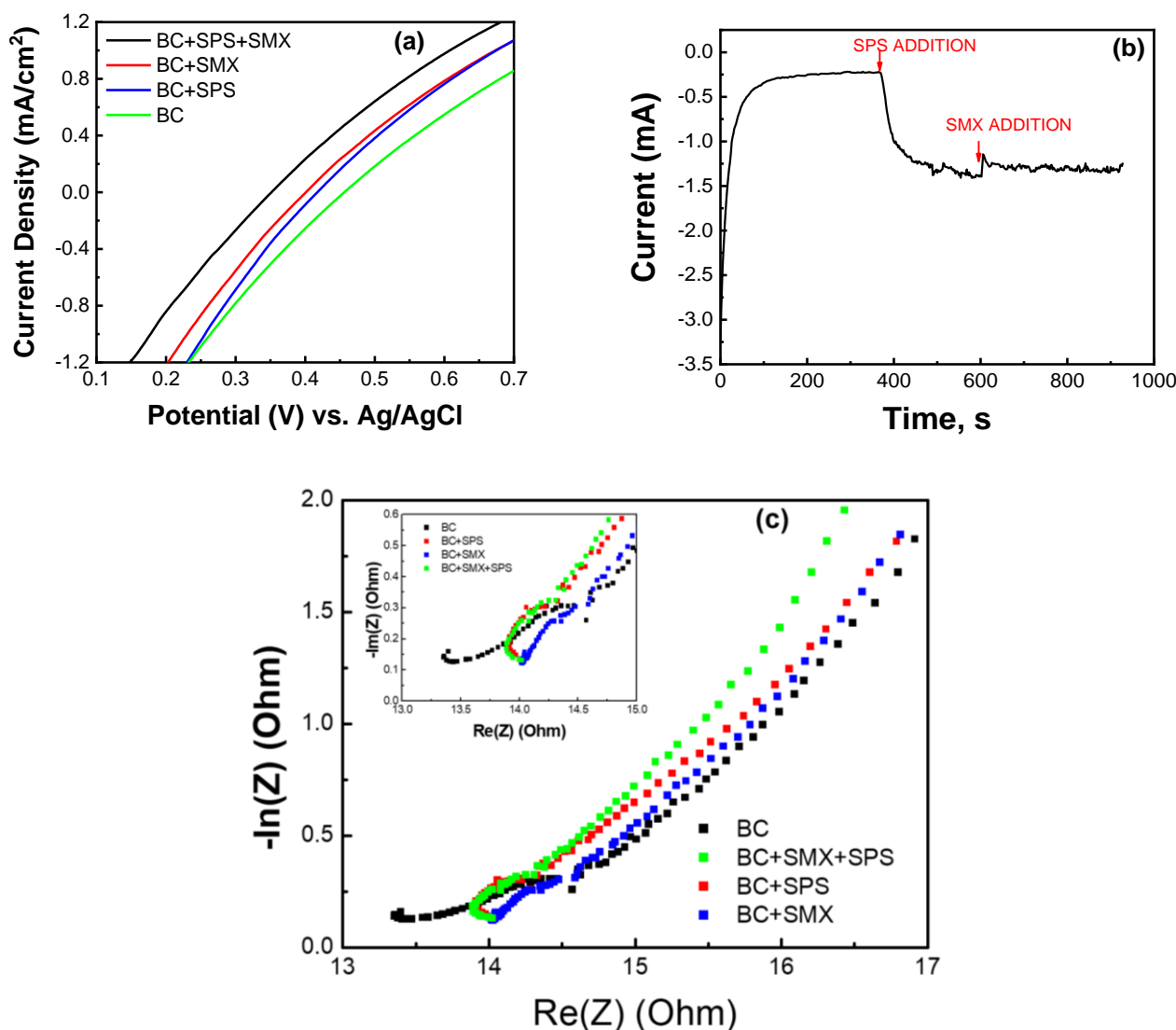
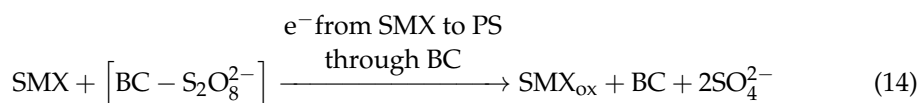
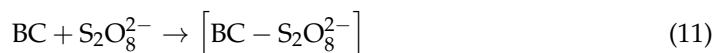


Figure 12. (a) LSV curves obtained under different conditions (SMX = 0.5 mg L⁻¹, SPS = 250 mg L⁻¹, Na₂SO₄ = 0.1 M); (b) I-t curves obtained at 0 V vs. Ag/AgCl (0.1 M Na₂SO₄); (c) EIS analysis of BC, BC/SPS, BC/SMX, and BC/SPS/SMX systems (SMX = 0.5 mg L⁻¹, SPS = 250 mg L⁻¹, Na₂SO₄ = 0.1 M).

In summary and based on the above analysis, the following electron transfer mechanism can be proposed in the BC/SPS system for the SMX decomposition:



where [BC-S₂O₈²⁻] symbolizes the BC-PS complex, BC_{OX} is the oxidation state of the biochar, and SMX_{OX} is the oxidized form of SMX and intermediates. The regions of the carbon surface characterized by high electron density contribute to the creation of

active centers, consequently initiating the interaction between biochar and SPS and finally resulting in the formation of surface-bound complexes (Equation (11)). This is followed by internal electron transfer within the complex (Equation (12)) and electron uptake into the SPS by SMX through the carbon structure of biochar (Equations (13) and (14)). Therefore, SMX oxidation is achieved, to a certain extent, regardless of the existence of active oxidizing species such as HO^\bullet , $\text{SO}_4^{\bullet-}$.

2.3.2. Effect of Scavengers

To estimate the radical pathway and the participation of singlet oxygen, $^1\text{O}_2$, [73], degradation experiments were conducted in the presence of 10 g L^{-1} methanol and *t*-butanol in large excess (i.e., alcohol to SMX ratio of 20,000) and 100 mg L^{-1} sodium azide [74,75]. In particular, methanol reacts with sulfate and hydroxyl radicals at a similar rate, while *t*-butanol reacts with hydroxyl radicals at a rate that is three times greater than with sulfate radicals [76,77]. To inhibit charge transfer via $^1\text{O}_2$, sodium azide was used as a quenching agent at a concentration equal to that of the biochar. Figure 13 shows that methanol does not practically affect degradation. On the contrary, SMX degradation was inhibited in the presence of *t*-butanol, implying that hydroxyl radicals were the dominant ones in the solution, while singlet oxygen may also participate in the oxidation process, since NaN_3 seems to slow degradation.

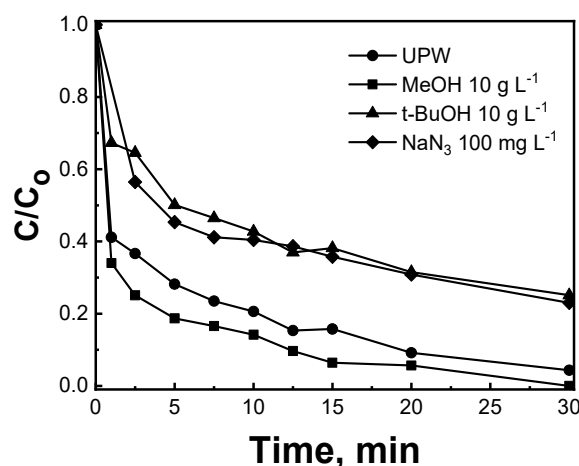


Figure 13. Effect of scavengers on the degradation of 0.5 mg L^{-1} SMX with 100 mg L^{-1} biochar and 250 mg L^{-1} SPS in UPW and inherent pH.

2.4. Biochar Reuse

To assess the stability of biochar upon repeated use, five consecutive runs were performed as follows: fresh biochar at 250 mg L^{-1} was mixed with 300 mg L^{-1} SPS and 0.5 mg L^{-1} SMX and the mixture was left to react for 30 min. The used biochar was removed by filtration, washed with UPW and reused in the following experiment and this cycle was repeated four times. The 30-min SMX conversion partly decreased from 100% in the first run to 85% in the fifth run, thus implying that the biochar can retain most of its activity although SPS may oxidize its surface according to the electron transfer mechanism discussed in Section 2.3.1. These results are in good agreement with previous studies reporting good stability of alike biochars [78].

3. Materials and Methods

3.1. Biochar Preparation

Branches of lemon tree were collected from the area of Patras, W. Greece, and lemon stalks were separated and dried in an oven at $105 \text{ }^\circ\text{C}$ for 2 d to remove moisture. The dried biomass was fragmented, weighed, and pyrolyzed at $850 \text{ }^\circ\text{C}$ using a cylindrical ceramic vessel (LH 60/12, Nabertherm GmbH, Lilienthal, Germany). The vessel was sealed with a ceramic lid to reduce oxygen by up to 20% of the quantity required for the complete

burning of biomass. The biochar mass obtained after pyrolysis was 26% of the starting biomass. Finally, the biochar was sieved, and the fraction with particles < 75 μm in diameter was used to conduct experiments. For preliminary runs, other parts of the lemon tree were also used to prepare biochar, e.g., leaves (pyrolyzed at 850 $^{\circ}\text{C}$ and 400 $^{\circ}\text{C}$) and branches (pyrolyzed at 850 $^{\circ}\text{C}$).

3.2. Biochar Characterization

The N_2 adsorption-desorption isotherms at liquid N_2 temperature were used for the determination of specific surface area (SSA) and pore size distribution (Tristar 3000 porosimeter, Micromeritics, Norcross, GA, USA). The point of zero charge was measured with the Potentiometric Mass titration technique (Tim Talk 8 Radiometer, Copenhagen, Denmark). A scanning electron microscope (SEM) (FEI Quanta 250 FEG, Hillsboro, OR, USA) worked under various pressures (10–4000 Pa). X-ray diffraction (XRD) patterns were recorded in a Bruker D8 (Billerica, MA, USA). An advance diffractometer was equipped with a nickel-filtered $\text{CuK}\alpha$ (1.5418 \AA) radiation source. Fourier transform infrared (FTIR) spectroscopy was performed using a Perkin Elmer Spectrum RX FTIR system (Waltham, MA, USA). The measurement range was 4000–400 cm^{-1} . More details about the characterization can be found in [79].

3.3. Electrode Preparation

Anodic materials for electrochemical measurements were prepared mixing 270 mg of biochar with 30 mg of carbon black; the latter was employed to achieve increased electrode stability and electrical conductivity. The mixture also had 100 mg PTFE added to guarantee the binding of the deposition material to the electrode surface. Ten mL of isopropanol was then added to the solid mixture under magnetic stirring, and this was subject to ultrasonic treatment for 30 min to dissolve PTFE. An electric mixer was operated for 10 min at 7000 rpm to establish a stable, homogenous suspension. Due to the mixture's insolubility in the solvent, the material was deposited on the carbon cloth using an electronic pipette, with the active electrode area being 9 cm^2 (3 cm \times 3 cm). To ensure successful deposition of the carbonaceous mixture on the organic substrate, the electrode was first placed into an oven at 105 $^{\circ}\text{C}$ for 15 min and then into a furnace at 340 $^{\circ}\text{C}$ for 20 min. The electrochemical characterization was performed with an Autolab potentiostat PGSTAT128N (Utrecht, The Netherlands). When needed, an Ag/AgCl electrode was used as a reference electrode.

3.4. Chemicals and Aqueous Matrices

Sulfamethoxazole (SMX, $\text{C}_{10}\text{H}_{11}\text{N}_3\text{O}_3\text{S}$, analytical standard, C.A.S. number: 723–46–6), Valsartan (VAL, $\text{C}_{24}\text{H}_{29}\text{N}_5\text{O}_3$ analytical standard, C.A.S. number: 137862-53-4), Losartan (LOS, $\text{C}_{22}\text{H}_{23}\text{ClN}_6\text{O}$ analytical standard, C.A.S. number: 114798-26-4), Dexamethasone (DEX, $\text{C}_{22}\text{H}_{29}\text{FO}_5$ analytical standard, C.A.S. number: 50-02-2), sodium persulfate (SPS, $\text{Na}_2\text{S}_2\text{O}_8$, 99 +%, C.A.S. number: 7775-27-1), sulfuric acid (H_2SO_4 , 95 wt%), sodium hydroxide (NaOH, 98 wt%), tert-butanol (t-BuOH, C.A.S. number: 75-65-0), methanol (MeOH, 99.9%, C.A.S. number: 67-56-1), sodium azide (NaN_3 , C.A.S. number: 26628-22-8), humic acid (HA, C.A.S. number: 1415-93-6), sodium chloride (NaCl, C.A.S. number: 7647-14-5), and sodium bicarbonate (NaHCO_3 , C.A.S. number: 144-55-8) were purchased from Sigma–Aldrich (St. Louis, MO, USA).

Most of the experiments were performed in ultrapure water (UPW, pH = 5.9, conductivity = 18.2 $\text{M}\Omega^{-1} \text{cm}^{-1}$), while other matrices included: (i) commercially available bottled water (brand name: ZAGORI) (BW, pH = 7.6, conductivity = 359 $\mu\text{S cm}^{-1}$, TDS = 260 mg L^{-1} , total hardness (CaCO_3) = 219 mg L^{-1} , Cl^- = 4.3 mg L^{-1} , SO_4^{2-} = 9.2 mg L^{-1} , HCO_3^- = 244 mg L^{-1} , NO_3^- = 1.93 mg L^{-1} , Mg^{2+} = 3.1 mg L^{-1} , Ca^{2+} = 83 mg L^{-1} , K^+ = 1 mg L^{-1} and Na^+ = 2.9 mg L^{-1}); (ii) seawater (SW) collected from a coastal area in Patras city, W. Greece; (iii) surface water collected from river Glafkos, Patras city, W. Greece (RW, pH = 8.1, conductivity = 283 $\mu\text{S cm}^{-1}$, TSS = 17 mg L^{-1} , VSS = 7 mg L^{-1} , COD = 3.8 mg L^{-1} , SO_4^{2-} = 8 mg L^{-1} , NO_3^- = 0.9 mg L^{-1} , Cl^- = 1 mg L^{-1} , NH_3 < 1 mg L^{-1});

and (iv) secondary effluent taken from the WWTP of University of Patras (WW, COD = 48.5 mg L⁻¹, TOC = 2.5 mg L⁻¹, TSS = 22 mg L⁻¹, HCO₃⁻ = 278 mg L⁻¹, Cl⁻ = 262.4 mg L⁻¹, PO₄³⁻ = 15 mg L⁻¹, Br⁻ = 165.6 mg L⁻¹, Ca²⁺ = 112 mg L⁻¹).

3.5. Experimental Procedure

A 50 mg L⁻¹ stock solution of SMX in UPW was used to prepare the working solutions at the desired concentration and matrix. Experiments were performed in a 250 mL beaker made of borosilicate glass, and the working volume was 120 mL under continuous magnetic stirring. Liquid samples of about 1.2 mL were withdrawn at regular intervals, then 0.3 mL of methanol was added to quench the reaction, and it was finally filtered with a 0.22 µm pore diameter filter (PVDF, Whatman). For those experiments performed at pH values other than the inherent, adjustment was done adding the appropriate volume of acid or alkali. A similar approach was followed with pharmaceuticals other than SMX.

Apparent rate constants were computed assuming that the oxidation follows a pseudo-first-order kinetic model:

$$\ln C = \ln C_0 - k_{\text{app}}t \quad (15)$$

where C and C_0 is SMX concentration at $t = t$ and $t = 0$, respectively, and k_{app} is the apparent rate constant.

3.6. Analytical Methods

SMX concentration was monitored with high-performance liquid chromatography using a Waters Alliance 2695 system equipped with (i) a gradient pump (Waters 2695, Milford, PA, USA), (ii) a photodiode array detector (Waters 2996, Milford, PA, USA), (iii) a Kinetex C18 100A column (150 × 3 mm; 2.6 µm particle size) (Phenomenex, Torrance, CA, USA) where separation was achieved, and (iv) a 0.5 µm inline filter (KrudKatcher Ultra, Phenomenex, Torrance, CA, USA). The elution of the kinetic phase was done isocratically at a flowrate of 0.25 mL min⁻¹ at 45 °C and consisted of 75% UPW (0.1% phosphoric acid) and 25% acetonitrile. The injection volume was 100 µL.

4. Conclusions

The valorization of citrus residues can produce carbonaceous materials, such as biochar, which can act as catalysts to activate persulfate and break down emerging micro-pollutants, such as antibiotics. In this work, a highly active and stable biochar was produced from lemon stalks through pyrolysis at 850 °C and used for the removal of sulfamethoxazole by adsorption/oxidation. The main conclusions are summarized as follows:

- (1) Biochar characterization by various techniques gives useful information regarding its composition, as well as its structural and electronic properties; such information can be related to its activity and associated mechanisms (i.e., radical and electron transfer) for persulfate activation and subsequent SMX degradation. Specifically, the biochar has a significant amount of calcium carbonate, moderate SSA, and a pzc value 9.2. A total of 100% degradation of SMX can be achieved under pH = 3, 100 mg L⁻¹ biochar, and 250 g L⁻¹ SPS.
- (2) Process efficiency is dictated by the interactions between the properties of the biochar, the organic pollutant, the oxidant source, and the water matrix. This interplay eventually determines the dominant reaction pathways and kinetics.
- (3) Although several operating variables may determine efficiency to various degrees, particular emphasis must be given to the water matrix effect; this usually is underestimated since studies are mainly performed at conditions that are not environmentally realistic.
- (4) The biochar can be applied in more realistic applications, although higher amounts of biochar may be needed.

Author Contributions: S.G., investigation, data curation; J.V., investigation, data curation, writing—original draft preparation; Z.F., validation, writing—review and editing; I.D.M., investigation; D.V., writing—review and editing.; S.G.P., writing—review and editing; D.M., writing—review and editing. All authors have read and agreed to the published version of the manuscript.

Funding: This research was funded by the Hellenic Foundation for Research and Innovation (H.F.R.I.) under the “First Call for H.F.R.I. Research Projects to support Faculty members and Researchers and the procurement of high-cost research equipment grant” (Project Number: 81080).

Data Availability Statement: The data presented in this study are available on request from the corresponding author.

Acknowledgments: S.G., J.V., D.V., and D.M. acknowledge support by the H.F.R.I.

Conflicts of Interest: The authors declare no conflict of interest.

References

1. Alduina, R. Antibiotics and Environment. *Antibiotics* **2020**, *9*, 202. [[CrossRef](#)]
2. Baran, W.; Sochacka, J.; Wardas, W. Toxicity and Biodegradability of Sulfonamides and Products of Their Photocatalytic Degradation in Aqueous Solutions. *Chemosphere* **2006**, *65*, 1295–1299. [[CrossRef](#)]
3. Deng, Y.; Li, B.; Zhang, T. Bacteria That Make a Meal of Sulfonamide Antibiotics: Blind Spots and Emerging Opportunities. *Environ. Sci. Technol.* **2018**, *52*, 3854–3868. [[CrossRef](#)]
4. Manzetti, S.; Ghisi, R. The Environmental Release and Fate of Antibiotics. *Mar. Pollut. Bull.* **2014**, *79*, 7–15. [[CrossRef](#)]
5. Thiele-Bruhn, D.S. *Environmental Risks from Mixtures of Antibiotic Pharmaceuticals in Soils—A Literature Review*; Umweltbundesamt: Dessau-Roßlau, Germany, 2019.
6. Kolpin, D.W.; Furlong, E.T.; Meyer, M.T.; Thurman, E.M.; Zaugg, S.D.; Barber, L.B.; Buxton, H.T. Pharmaceuticals, Hormones, and Other Organic Wastewater Contaminants in U.S. Streams, 1999–2000: A National Reconnaissance. *Environ. Sci. Technol.* **2002**, *36*, 1202–1211. [[CrossRef](#)]
7. Bernot, M.J.; Smith, L.; Frey, J. Human and Veterinary Pharmaceutical Abundance and Transport in a Rural Central Indiana Stream Influenced by Confined Animal Feeding Operations (CAFOs). *Sci. Total Environ.* **2013**, *445–446*, 219–230. [[CrossRef](#)]
8. Iglesias, A.; Nebot, C.; Vázquez, B.I.; Miranda, J.M.; Abuín, C.M.F.; Cepeda, A. Detection of Veterinary Drug Residues in Surface Waters Collected Nearby Farming Areas in Galicia, North of Spain. *Environ. Sci. Pollut. Res.* **2014**, *21*, 2367–2377. [[CrossRef](#)]
9. Veach, A.M.; Bernot, M.J. Temporal Variation of Pharmaceuticals in an Urban and Agriculturally Influenced Stream. *Sci. Total Environ.* **2011**, *409*, 4553–4563. [[CrossRef](#)]
10. Hruska, K.; Franek, M. Sulfonamides in the Environment: A Review and a Case Report. *Veterinární Medicína* **2012**, *57*, 1–35. [[CrossRef](#)]
11. Grenni, P.; Ancona, V.; Barra Caracciolo, A. Ecological Effects of Antibiotics on Natural Ecosystems: A Review. *Microchem. J.* **2018**, *136*, 25–39. [[CrossRef](#)]
12. Matongo, S.; Birungi, G.; Moodley, B.; Ndungu, P. Occurrence of Selected Pharmaceuticals in Water and Sediment of Umgeni River, KwaZulu-Natal, South Africa. *Environ. Sci. Pollut. Res.* **2015**, *22*, 10298–10308. [[CrossRef](#)]
13. Peng, X.; Tan, J.; Tang, C.; Yu, Y.; Wang, Z. Multiresidue determination of fluoroquinolone, sulfonamide, trimethoprim, and chloramphenicol antibiotics in urban waters in china. *Environ. Toxicol. Chem.* **2008**, *27*, 73. [[CrossRef](#)]
14. Yargeau, V.; Lopata, A.; Metcalfe, C. Pharmaceuticals in the Yamaska River, Quebec, Canada. *Water Qual. Res. J.* **2007**, *42*, 231–239. [[CrossRef](#)]
15. Tamtam, F.; Mercier, F.; Le Bot, B.; Eurin, J.; Tuc Dinh, Q.; Clément, M.; Chevreuil, M. Occurrence and Fate of Antibiotics in the Seine River in Various Hydrological Conditions. *Sci. Total Environ.* **2008**, *393*, 84–95. [[CrossRef](#)]
16. Barnes, K.K.; Kolpin, D.W.; Furlong, E.T.; Zaugg, S.D.; Meyer, M.T.; Barber, L.B. A National Reconnaissance of Pharmaceuticals and Other Organic Wastewater Contaminants in the United States—I) Groundwater. *Sci. Total Environ.* **2008**, *402*, 192–200. [[CrossRef](#)]
17. Qu, J.; Fan, M. The Current State of Water Quality and Technology Development for Water Pollution Control in China. *Crit. Rev. Environ. Sci. Technol.* **2010**, *40*, 519–560. [[CrossRef](#)]
18. Zheng, X.; Zhang, B.-T.; Teng, Y. Distribution of Phthalate Acid Esters in Lakes of Beijing and Its Relationship with Anthropogenic Activities. *Sci. Total Environ.* **2014**, *476–477*, 107–113. [[CrossRef](#)]
19. Zhang, B.-T.; Zhao, L.-X.; Lin, J.-M. Study on Superoxide and Hydroxyl Radicals Generated in Indirect Electrochemical Oxidation by Chemiluminescence and UV-Visible Spectra. *J. Environ. Sci.* **2008**, *20*, 1006–1011. [[CrossRef](#)]
20. Shukla, P.; Sun, H.; Wang, S.; Ang, H.M.; Tade, M.O. Co-SBA-15 for Heterogeneous Oxidation of Phenol with Sulfate Radical for Wastewater Treatment. *Catal. Today* **2011**, *175*, 380–385. [[CrossRef](#)]
21. Anipsitakis, G.P.; Dionysiou, D.D. Radical Generation by the Interaction of Transition Metals with Common Oxidants. *Environ. Sci. Technol.* **2004**, *38*, 3705–3712. [[CrossRef](#)]
22. Anipsitakis, G.P.; Dionysiou, D.D. Degradation of Organic Contaminants in Water with Sulfate Radicals Generated by the Conjunction of Peroxymonosulfate with Cobalt. *Environ. Sci. Technol.* **2003**, *37*, 4790–4797. [[CrossRef](#)]

23. Zhang, B.-T.; Zhao, L.; Lin, J.-M. Determination of Folic Acid by Chemiluminescence Based on Peroxomonosulfate-Cobalt(II) System. *Talanta* **2008**, *74*, 1154–1159. [[CrossRef](#)] [[PubMed](#)]
24. Zhang, B.-T.; Lin, J.-M. Chemiluminescence and Energy Transfer Mechanism of Lanthanide Ions in Different Media Based on Peroxomonosulfate System. *Luminescence* **2010**, *25*, 322–327. [[CrossRef](#)] [[PubMed](#)]
25. Liang, C.J.; Bruell, C.J.; Marley, M.C.; Sperry, K.L. Thermally Activated Persulfate Oxidation of Trichloroethylene (T.C.E.) and 1,1,1-Trichloroethane (T.C.A.) in Aqueous Systems and Soil Slurries. *Soil Sediment Contam. Int. J.* **2003**, *12*, 207–228. [[CrossRef](#)]
26. Ioannidi, A.; Arvaniti, O.S.; Nika, M.-C.; Aalizadeh, R.; Thomaidis, N.S.; Mantzavinos, D.; Frontistis, Z. Removal of Drug Losartan in Environmental Aquatic Matrices by Heat-Activated Persulfate: Kinetics, Transformation Products and Synergistic Effects. *Chemosphere* **2022**, *287*, 131952. [[CrossRef](#)]
27. Darsinou, B.; Frontistis, Z.; Antonopoulou, M.; Konstantinou, I.; Mantzavinos, D. Sono-Activated Persulfate Oxidation of Bisphenol A: Kinetics, Pathways and the Controversial Role of Temperature. *Chem. Eng. J.* **2015**, *280*, 623–633. [[CrossRef](#)]
28. Giannakopoulos, S.; Frontistis, Z.; Vakros, J.; Pouloupoulos, S.G.; Manariotis, I.D.; Mantzavinos, D. Combined Activation of Persulfate by Biochars and Artificial Light for the Degradation of Sulfamethoxazole in Aqueous Matrices. *J. Taiwan Inst. Chem. Eng.* **2022**, *136*, 104440. [[CrossRef](#)]
29. Xiang, Y.; Yang, K.; Zhai, Z.; Zhao, T.; Yuan, D.; Jiao, T.; Zhang, Q.; Tang, S. Molybdenum co-catalytic promotion for Fe³⁺/peroxydisulfate process: Performance, mechanism, and immobilization. *Chem. Eng. J.* **2022**, *438*, 135656. [[CrossRef](#)]
30. Pan, S.; Zhai, Z.; Yang, K.; Xiang, Y.; Tang, S.; Zhang, Y.; Jiao, T.; Zhang, Q.; Yuan, D. β -Lactoglobulin amyloid fibrils supported Fe(III) to activate peroxydisulfate for organic pollutants elimination. *Sep. Purif. Technol.* **2022**, *289*, 120806. [[CrossRef](#)]
31. Xiang, Y.; Liu, H.; Zhu, E.; Yang, K.; Yuan, D.; Jiao, T.; Zhang, Q.; Tang, S. Application of inorganic materials as heterogeneous cocatalyst in Fenton/Fenton-like processes for wastewater treatment. *Sep. Purif. Technol.* **2022**, *295*, 121293. [[CrossRef](#)]
32. Giannakopoulos, S.; Vakros, J.; Dracopoulos, V.; Manariotis, I.D.; Mantzavinos, D.; Lianos, P. Enhancement of the Photoelectrocatalytic Degradation Rate of a Pollutant in the Presence of a Supercapacitor. *J. Clean. Prod.* **2022**, *377*, 134456. [[CrossRef](#)]
33. Srivatsav, P.; Bhargav, B.S.; Shanmugasundaram, V.; Arun, J.; Gopinath, K.P.; Bhatnagar, A. Biochar as an Eco-Friendly and Economical Adsorbent for the Removal of Colorants (Dyes) from Aqueous Environment: A Review. *Water* **2020**, *12*, 3561. [[CrossRef](#)]
34. Ntaflou, M.; Vakros, J. Transesterification Activity of Modified Biochars from Spent Malt Rootlets Using Triacetin. *J. Clean. Prod.* **2020**, *259*, 120931. [[CrossRef](#)]
35. Azargohar, R.; Dalai, A.K. Steam and K.O.H. Activation of Biochar: Experimental and Modeling Studies. *Microporous Mesoporous Mater.* **2008**, *110*, 413–421. [[CrossRef](#)]
36. Kong, S.-H.; Loh, S.-K.; Bachmann, R.T.; Rahim, S.A.; Salimon, J. Biochar from Oil Palm Biomass: A Review of Its Potential and Challenges. *Renew. Sustain. Energy Rev.* **2014**, *39*, 729–739. [[CrossRef](#)]
37. Sharma, A.; Pareek, V.; Zhang, D. Biomass Pyrolysis—A Review of Modelling, Process Parameters and Catalytic Studies. *Renew. Sustain. Energy Rev.* **2015**, *50*, 1081–1096. [[CrossRef](#)]
38. *Renewable Energy Sources: Engineering, Technology, Innovation: I.C.O.R.E.S. 2017*; Mudryk, K.; Werle, S. (Eds.) Springer Proceedings in Energy; Springer International Publishing: Cham, Switzerland, 2018; ISBN 978-3-319-72370-9.
39. Fresh Lemons and Limes: Leading Producers Worldwide 2021. Statista. Available online: <https://www.statista.com/statistics/1045016/world-lemons-and-limes-major-producers/> (accessed on 24 August 2021).
40. Lykoudi, A.; Frontistis, Z.; Vakros, J.; Manariotis, I.D.; Mantzavinos, D. Degradation of Sulfamethoxazole with Persulfate Using Spent Coffee Grounds Biochar as Activator. *J. Environ. Manage.* **2020**, *271*, 111022. [[CrossRef](#)]
41. Magioglou, E.; Frontistis, Z.; Vakros, J.; Manariotis, I.; Mantzavinos, D. Activation of Persulfate by Biochars from Valorized Olive Stones for the Degradation of Sulfamethoxazole. *Catalysts* **2019**, *9*, 419. [[CrossRef](#)]
42. Kemmou, L.; Frontistis, Z.; Vakros, J.; Manariotis, I.D.; Mantzavinos, D. Degradation of Antibiotic Sulfamethoxazole by Biochar-Activated Persulfate: Factors Affecting the Activation and Degradation Processes. *Catal. Today* **2018**, *313*, 128–133. [[CrossRef](#)]
43. Avramiotis, E.; Frontistis, Z.; Manariotis, I.D.; Vakros, J.; Mantzavinos, D. Oxidation of Sulfamethoxazole by Rice Husk Biochar-Activated Persulfate. *Catalysts* **2021**, *11*, 850. [[CrossRef](#)]
44. Andrade, T.S.; Vakros, J.; Mantzavinos, D.; Lianos, P. Biochar Obtained by Carbonization of Spent Coffee Grounds and Its Application in the Construction of an Energy Storage Device. *Chem. Eng. J. Adv.* **2020**, *4*, 100061. [[CrossRef](#)]
45. Gao, G.; Cheong, L.-Z.; Wang, D.; Shen, C. Pyrolytic Carbon Derived from Spent Coffee Grounds as Anode for Sodium-Ion Batteries. *Carbon Resour. Convers.* **2018**, *1*, 104–108. [[CrossRef](#)]
46. Bourikas, K.; Vakros, J.; Kordulis, C.; Lycourghiotis, A. Potentiometric Mass Titrations: Experimental and Theoretical Establishment of a New Technique for Determining the Point of Zero Charge (P.Z.C.) of Metal (Hydr)Oxides. *J. Phys. Chem. B* **2003**, *107*, 9441–9451. [[CrossRef](#)]
47. Mroziak, W.; Minofar, B.; Thongsamer, T.; Wiriyaiphong, N.; Khawkomol, S.; Plaimart, J.; Vakros, J.; Karapanagioti, H.; Vinitnatharat, S.; Werner, D. Valorisation of agricultural waste derived biochars in aquaculture to remove organic micropollutants from water—Experimental study and molecular dynamics simulations. *J. Environ. Manage.* **2021**, *300*, 113717. [[CrossRef](#)] [[PubMed](#)]
48. Grilla, E.; Vakros, J.; Konstantinou, I.; Manariotis, I.D.; Mantzavinos, D. Activation of persulfate by biochar from spent malt rootlets for the degradation of trimethoprim in the presence of inorganic ions. *J. Chem. Technol. Biotechnol.* **2020**, *95*, 2348–2358. [[CrossRef](#)]

49. Fang, G.; Wu, W.; Liu, C.; Dionysiou, D.D.; Deng, Y.; Zhou, D. Activation of Persulfate with Vanadium Species for P.C.B.s Degradation: A Mechanistic Study. *Appl. Catal. B Environ.* **2017**, *202*, 1–11. [[CrossRef](#)]
50. Avisar, D.; Primor, O.; Gozlan, I.; Mamane, H. Sorption of Sulfonamides and Tetracyclines to Montmorillonite Clay. *Water. Air. Soil Pollut.* **2010**, *209*, 439–450. [[CrossRef](#)]
51. Ribeiro, R.S.; Frontistis, Z.; Mantzavinos, D.; Silva, A.M.T.; Faria, J.L.; Gomes, H.T. Screening of Heterogeneous Catalysts for the Activated Persulfate Oxidation of Sulfamethoxazole in Aqueous Matrices. Does the Matrix Affect the Selection of Catalyst? *J. Chem. Technol. Biotechnol.* **2019**, *8*, 2425–2432. [[CrossRef](#)]
52. Wang, Y.; Cao, D.; Zhao, X. Heterogeneous Degradation of Refractory Pollutants by Peroxymonosulfate Activated by CoOx-Doped Ordered Mesoporous Carbon. *Chem. Eng. J.* **2017**, *328*, 1112–1121. [[CrossRef](#)]
53. Chen, L.; Zuo, X.; Yang, S.; Cai, T.; Ding, D. Rational Design and Synthesis of Hollow Co₃O₄@Fe₂O₃ Core-Shell Nanostructure for the Catalytic Degradation of Norfloxacin by Coupling with Peroxymonosulfate. *Chem. Eng. J.* **2019**, *359*, 373–384. [[CrossRef](#)]
54. Lai, L.; Yan, J.; Li, J.; Lai, B. Co/Al₂O₃-EPM as Peroxymonosulfate Activator for Sulfamethoxazole Removal: Performance, Biototoxicity, Degradation Pathways and Mechanism. *Chem. Eng. J.* **2018**, *343*, 676–688. [[CrossRef](#)]
55. Serna-Galvis, E.A.; Jojoa-Sierra, S.D.; Berrio-Perlaza, K.E.; Ferraro, F.; Torres-Palma, R.A. Structure-Reactivity Relationship in the Degradation of Three Representative Fluoroquinolone Antibiotics in Water by Electrogenerated Active Chlorine. *Chem. Eng. J.* **2017**, *315*, 552–561. [[CrossRef](#)]
56. Ao, X.; Liu, W.; Sun, W.; Cai, M.; Ye, Z.; Yang, C.; Lu, Z.; Li, C. Medium Pressure UV-Activated Peroxymonosulfate for Ciprofloxacin Degradation: Kinetics, Mechanism, and Genotoxicity. *Chem. Eng. J.* **2018**, *345*, 87–97. [[CrossRef](#)]
57. Sichel, C.; Garcia, C.; Andre, K. Feasibility Studies: U.V./Chlorine Advanced Oxidation Treatment for the Removal of Emerging Contaminants. *Water Res.* **2011**, *45*, 6371–6380. [[CrossRef](#)]
58. Li, A.; Wu, Z.; Wang, T.; Hou, S.; Huang, B.; Kong, X.; Li, X.; Guan, Y.; Qiu, R.; Fang, J. Kinetics and Mechanisms of the Degradation of P.P.C.P.s by Zero-Valent Iron (Fe⁰) Activated Peroxydisulfate (P.D.S.) System in Groundwater. *J. Hazard. Mater.* **2018**, *357*, 207–216. [[CrossRef](#)]
59. Xiao, S.; Cheng, M.; Zhong, H.; Liu, Z.; Liu, Y.; Yang, X.; Liang, Q. Iron-Mediated Activation of Persulfate and Peroxymonosulfate in Both Homogeneous and Heterogeneous Ways: A Review. *Chem. Eng. J.* **2020**, *384*, 123265. [[CrossRef](#)]
60. Ashfaq, M.; Li, Y.; Wang, Y.; Chen, W.; Wang, H.; Chen, X.; Wu, W.; Huang, Z.; Yu, C.-P.; Sun, Q. Occurrence, Fate, and Mass Balance of Different Classes of Pharmaceuticals and Personal Care Products in an Anaerobic-Anoxic-Oxic Wastewater Treatment Plant in Xiamen, China. *Water Res.* **2017**, *123*, 655–667. [[CrossRef](#)]
61. Botero-Coy, A.M.; Martínez-Pachón, D.; Boix, C.; Rincón, R.J.; Castillo, N.; Arias-Marín, L.P.; Manrique-Losada, L.; Torres-Palma, R.; Moncayo-Lasso, A.; Hernández, F. An Investigation into the Occurrence and Removal of Pharmaceuticals in Colombian Wastewater. *Sci. Total Environ.* **2018**, *642*, 842–853. [[CrossRef](#)]
62. Casado, J.; Rodríguez, I.; Ramil, M.; Cela, R. Selective Determination of Antimycotic Drugs in Environmental Water Samples by Mixed-Mode Solid-Phase Extraction and Liquid Chromatography Quadrupole Time-of-Flight Mass Spectrometry. *J. Chromatogr. A* **2014**, *1339*, 42–49. [[CrossRef](#)]
63. Azuma, T.; Otomo, K.; Kunitou, M.; Shimizu, M.; Hosomaru, K.; Mikata, S.; Ishida, M.; Hisamatsu, K.; Yunoki, A.; Mino, Y.; et al. Environmental Fate of Pharmaceutical Compounds and Antimicrobial-Resistant Bacteria in Hospital Effluents, and Contributions to Pollutant Loads in the Surface Waters in Japan. *Sci. Total Environ.* **2019**, *657*, 476–484. [[CrossRef](#)]
64. Mandaric, L.; Diamantini, E.; Stella, E.; Cano-Paoli, K.; Valle-Sistac, J.; Molins-Delgado, D.; Bellin, A.; Chiogna, G.; Majone, B.; Diaz-Cruz, M.S.; et al. Contamination Sources and Distribution Patterns of Pharmaceuticals and Personal Care Products in Alpine Rivers Strongly Affected by Tourism. *Sci. Total Environ.* **2017**, *590–591*, 484–494. [[CrossRef](#)]
65. Cortez, F.S.; Souza, L.D.S.; Guimarães, L.L.; Almeida, J.E.; Pusceddu, F.H.; Maranhão, L.A.; Mota, L.G.; Nobre, C.R.; Moreno, B.B.; Abessa, D.M.D.S. et al. Ecotoxicological Effects of Losartan on the Brown Mussel *Perna Perna* and Its Occurrence in Seawater from Santos Bay (Brazil). *Sci. Total Environ.* **2018**, *637–638*, 1363–1371. [[CrossRef](#)] [[PubMed](#)]
66. Arvaniti, O.S.; Bairamis, F.; Konstantinou, I.; Mantzavinos, D.; Frontistis, Z. Degradation of Antihypertensive Drug Valsartan in Water Matrices by Heat and Heat/Ultrasound Activated Persulfate: Kinetics, Synergy Effect and Transformation Products. *Chem. Eng. J. Adv.* **2020**, *4*, 100062. [[CrossRef](#)]
67. Martínez-Pachón, D.; Ibáñez, M.; Hernández, F.; Torres-Palma, R.A.; Moncayo-Lasso, A. Photo-Electro-Fenton Process Applied to the Degradation of Valsartan: Effect of Parameters, Identification of Degradation Routes and Mineralization in Combination with a Biological System. *J. Environ. Chem. Eng.* **2018**, *6*, 7302–7311. [[CrossRef](#)]
68. Dasenaki, M.E.; Thomaidis, N.S. Multianalyte Method for the Determination of Pharmaceuticals in Wastewater Samples Using Solid-Phase Extraction and Liquid Chromatography-Tandem Mass Spectrometry. *Anal. Bioanal. Chem.* **2015**, *407*, 4229–4245. [[CrossRef](#)]
69. Mohseni, S.N.; Amooey, A.A.; Tashakkorian, H.; Amouei, A.I. Removal of Dexamethasone from Aqueous Solutions Using Modified Clinoptilolite Zeolite (Equilibrium and Kinetic). *Int. J. Environ. Sci. Technol.* **2016**, *13*, 2261–2268. [[CrossRef](#)]
70. Ioannidi, A.A.; Vakros, J.; Frontistis, Z.; Mantzavinos, D. Tailoring the Biochar Physicochemical Properties Using a Friendly Eco-Method and Its Application on the Oxidation of the Drug Losartan through Persulfate Activation. *Catalysts* **2022**, *12*, 1245. [[CrossRef](#)]

71. Li, M.; Bi, G.Y.; Xiang, L.; Chen, X.T.; Qin, Y.J.; Mo, C.H.; Zhou, S.Q. Improved cathodic oxygen reduction and bioelectricity generation of electrochemical reactor based on reduced graphene oxide decorated with titanium-based composites. *Bioresour. Techn.* **2020**, *296*, 122319. [[CrossRef](#)]
72. Yang, Z.; Wang, Z.; Liang, G.; Zhang, X.; Xie, X. Catalyst Bridging-Mediated Electron Transfer for Nonradical Degradation of Bisphenol A via Natural Manganese Ore-Cornstalk Biochar Composite Activated Peroxymonosulfate. *Chem. Eng. J.* **2021**, *426*, 131777. [[CrossRef](#)]
73. Yun, E.-T.; Yoo, H.-Y.; Bae, H.; Kim, H.-I.; Lee, J. Exploring the Role of Persulfate in the Activation Process: Radical Precursor Versus Electron Acceptor. *Environ. Sci. Technol.* **2017**, *51*, 10090–10099. [[CrossRef](#)]
74. Li, M.; Li, Z.; Yu, X.; Wu, Y.; Mo, C.; Luo, M.; Li, L.; Zhou, S.; Liu, Q.; Wang, N.; et al. FeN₄-doped carbon nanotubes derived from metal organic frameworks for effective degradation of organic dyes by peroxymonosulfate: Impacts of FeN₄ spin states. *Chem. Eng. J.* **2022**, *431*, 133339. [[CrossRef](#)]
75. Li, M.; Mo, C.H.; Luo, X.; He, K.Y.; Yan, J.F.; Wu, Q.; Yu, P.F.; Han, W.; Feng, N.X.; Yeung, K.L.; et al. Exploring key reaction sites and deep degradation mechanism of perfluorooctane sulfonate via peroxymonosulfate activation under electrocoagulation process. *Water Res.* **2021**, *207*, 117849. [[CrossRef](#)] [[PubMed](#)]
76. Yin, R.; Guo, W.; Wang, H.; Du, J.; Wu, Q.; Chang, J.-S.; Ren, N. Singlet Oxygen-Dominated Peroxydisulfate Activation by Sludge-Derived Biochar for Sulfamethoxazole Degradation through a Nonradical Oxidation Pathway: Performance and Mechanism. *Chem. Eng. J.* **2019**, *357*, 589–599. [[CrossRef](#)]
77. Yu, J.; Tang, L.; Pang, Y.; Zeng, G.; Wang, J.; Deng, Y.; Liu, Y.; Feng, H.; Chen, S.; Ren, X. Magnetic Nitrogen-Doped Sludge-Derived Biochar Catalysts for Persulfate Activation: Internal Electron Transfer Mechanism. *Chem. Eng. J.* **2019**, *364*, 146–159. [[CrossRef](#)]
78. Ntzoufra, P.; Vakros, J.; Frontistis, Z.; Tsatsos, S.; Kyriakou, G.; Kennou, S.; Manariotis, I.D.; Mantzavinos, D. Effect of Sodium Persulfate Treatment on the Physicochemical Properties and Catalytic Activity of Biochar Prepared from Spent Malt Rootlets. *J. Environ. Chem. Eng.* **2021**, *9*, 105071. [[CrossRef](#)]
79. Avramiotis, E.; Frontistis, Z.; Manariotis, I.D.; Vakros, J.; Mantzavinos, D. On the Performance of a Sustainable Rice Husk Biochar for the Activation of Persulfate and the Degradation of Antibiotics. *Catalysts* **2021**, *11*, 1303. [[CrossRef](#)]

Disclaimer/Publisher's Note: The statements, opinions and data contained in all publications are solely those of the individual author(s) and contributor(s) and not of MDPI and/or the editor(s). MDPI and/or the editor(s) disclaim responsibility for any injury to people or property resulting from any ideas, methods, instructions or products referred to in the content.